Observational constraints and dynamical analysis of Kaniadakis horizon-entropy cosmology

A. Hernández-Almada [ID],[1]* Genly Leon [ID],[2,3] Juan Magaña [ID],[4] Miguel A. García-Aspeitia [ID],[5] V. Motta [ID],[6] Emmanuel N. Saridakis [ID],[7,8,9] Kuralay Yesmakhanova [ID][9,10] and Alfredo D. Millano [ID][2]

[1]*Facultad de Ingeniería, Universidad Autónoma de Querétaro, Centro Universitario Cerro de las Campanas, 76010 Santiago de Querétaro, México*
[2]*Departamento de Matemáticas, Universidad Católica del Norte, Avda. Angamos 0610, Casilla 1280, Antofagasta, Chile*
[3]*Institute of Systems Science, Durban University of Technology, PO Box 1334, Durban 4000, South Africa*
[4]*Instituto de Astrofísica and Centro de Astro-Ingeniería, Pontificia Universidad Católica de Chile, Av. Vicuña Mackenna 4860, Santiago, Chile*
[5]*Departamento de Física y Matemáticas, Universidad Iberoamericana Ciudad de México, Prolongación Paseo de la Reforma 880, México D. F. 01219, México*
[6]*Instituto de Física y Astronomía, Facultad de Ciencias, Universidad de Valparaíso, Avda. Gran Bretaña 1111, Valparaíso, Chile*
[7]*Institute for Astronomy, Astrophysics, Space Applications and Remote Sensing, National Observatory of Athens, Lofos Nymfon, 11852 Athens, Greece*
[8]*CAS Key Laboratory for Researches in Galaxies and Cosmology, Department of Astronomy, University of Science and Technology of China, Hefei, Anhui 230026, P. R. China*
[9]*Ratbay Myrzakulov Eurasian International Centre for Theoretical Physics, Nur-Sultan 010009, Kazakhstan*
[10]*Ratbay Myrzakulov Eurasian International Centre for Theoretical Physics, Eurasian National University, Nur-Sultan Astana 010008, Kazakhstan*

ABSTRACT

We study the scenario of Kaniadakis horizon-entropy cosmology, which arises from the application of the gravity-thermodynamics conjecture using the Kaniadakis modified entropy. The resulting modified Friedmann equations contain extra terms that constitute an effective dark energy sector. We use data from cosmic chronometers, Type Ia supernova, H II galaxies, strong lensing systems, and baryon acoustic oscillation observations, and we apply a Bayesian Markov chain Monte Carlo analysis to construct the likelihood contours for the model parameters. We find that the Kaniadakis parameter is constrained around 0, namely around the value where the standard Bekenstein–Hawking is recovered. Concerning the normalized Hubble parameter, we find $h = 0.708^{+0.012}_{-0.011}$, a result that is independently verified by applying the $\mathbb{H}0(z)$ diagnostic and, thus, we conclude that the scenario at hand can alleviate the H_0 tension problem. Regarding the transition redshift, the reconstruction of the cosmographic parameters gives $z_{\mathrm{T}} = 0.715^{+0.042}_{-0.041}$. Furthermore, we apply the Akaike, Bayesian, and deviance information criteria, and we find that in most data sets the scenario is statistical equivalent to Λ cold dark matter one. Moreover, we examine the big bang nucleosynthesis, and we show that the scenario satisfies the corresponding requirements. Additionally, we perform a phase-space analysis, and we show that the Universe past attractor is the matter-dominated epoch, while at late times the Universe results in the dark-energy-dominated solution. Finally, we show that Kaniadakis horizon-entropy cosmology accepts heteroclinic sequences, but it cannot exhibit bounce and turnaround solutions.

Key words: cosmological parameters – dark energy.

1 INTRODUCTION

Cosmology is one of the most exciting adventures in the human endeavour: the understanding of the origin, evolution, and future of our Universe by combining the physics at micro- and macro-scales in a joint framework. In particular, the Universe acceleration is one of the most important puzzles. Discovered by the Supernovae team, through Type Ia supernovae (SNIa; Riess et al. 1998), it is also confirmed by the acoustic peaks of the cosmic microwave background (CMB) radiation (Spergel et al. 2003), and recently tested with large-scale structure measurements (Nadathur et al. 2020). Tackling the Universe acceleration is indeed a complicated issue due to the attractive nature of gravity in the general relativity (GR) framework. The first approach on its explanation is through

the addition of the cosmological constant (CC; Carroll 2001). Thus, using the continuity equation and assuming a constant energy density ($\dot{\rho} = 0$), it is possible to conclude that the equation of state (EoS) is $w = -1$, which is in concordance with what is expected for a fluid that accelerates the Universe. Another main characteristic is that the energy density of the CC must be subdominant in order to obtain a late and non-violent acceleration. From the quantum field theory viewpoint, the CC can be explained by the addition of quantum vacuum fluctuations (QVF) associated with the space–time. Therefore, the expansion of space–time implies an increase of QVF, maintaining a constant energy density. However, when we calculate the energy density of the QVF, the result is in complete disagreement with the observed one (see Zel'dovich, Krasinski & Zeldovich 1968; Weinberg 1989), this is the so-called *fine tuning problem* (Addazi et al. 2021). In addition to the CC problem, a 4.2σ tension in the current Hubble parameter value (H_0) measured by Supernova H_0 for the Equation of State (SH0ES) collaboration (Riess et al. 2021) and

* E-mail: ahalmada@uaq.mx

the one obtained by Planck collaboration under the Λ cold dark matter (ΛCDM) scenario (Aghanim et al. 2020) has been recently observed.

The above-mentioned problem that afflicts the understanding of the CC in this framework has driven the community to propose other approaches like scalar fields, dynamical dark energy, viscous fluids, Chaplygin gas (Hernández-Almada et al. 2019) or modifications to GR such as unimodular gravity (García-Aspeitia et al. 2019, 2021), Einstein–Gauss–Bonnet (García-Aspeitia & Hernández-Almada 2021), Brane Worlds (Garcia-Aspeitia et al. 2018), among others (see Motta et al. 2021; Saridakis et al. 2021, for a compilation of the mentioned previous models). Despite the fact that we can have numerous models and scenarios describing the late-time acceleration, at the end of the day, the detailed confrontation with observations, alongside theoretical consistency, will be the main method for their validation.

One interesting alternative to investigate the dynamics of the Universe is the gravity-thermodynamics approach (Jacobson 1995; Padmanabhan 2005, 2010). This takes advantage of the first law of thermodynamics and the standard Bekenstein–Hawking entropy–area relation for black holes, which applied to the apparent cosmological horizon leads to the Friedmann equations (Frolov & Kofman 2003; Cai & Kim 2005; Akbar & Cai 2007; Cai & Cao 2007). Hence, the application of this conjecture with various alternative entropy relations leads to modified Friedmann equations whose additional terms can source the cosmic acceleration (Akbar & Cai 2006; Paranjape, Sarkar & Padmanabhan 2006; Cai & Cao 2007; Sheykhi, Wang & Cai 2007; Cai & Ohta 2010; Jamil, Saridakis & Setare 2010a,b; Sheykhi 2010a,b, 2018; Wang et al. 2010; Gim, Kim & Yi 2014; Fan & Lu 2015; Lymperis & Saridakis 2018; Saridakis 2020).

One interesting class of extended entropies arises through generalizations for the Boltzmann–Gibbs statistics. In particular, one modifies the classical entropy of a system given by $S = -k_B \sum_i p_i \ln p_i$, where p_i is the probability of a system to be within a microstate, through a non-extensive analysis resulting into the Tsallis entropy (Tsallis 1988; Lyra & Tsallis 1998), through quantum-gravitational considerations resulting into Barrow entropy (Barrow 2020), or through relativistic extensions resulting into Kaniadakis entropy (Kaniadakis 2002, 2005). Hence, the application of the gravity-thermodynamics conjecture using the above-modified horizon entropy gives rise to modified cosmological scenarios. In Lymperis & Saridakis (2018), this was performed in the framework of Tsallis entropy, in Saridakis (2020), Saridakis & Basilakos (2021), Leon et al. (2021), and Barrow, Basilakos & Saridakis (2021), it was applied for the Barrow entropy case, and recently (Lymperis, Basilakos & Saridakis 2021), it was used in the Kaniadakis entropy frame.

In this work, we investigate Kaniadakis horizon-entropy cosmology by confronting it to observational data from cosmic chronometers, SNIa, H II galaxies (HIIG), strong lensing systems (SLSs), and baryon acoustic oscillation (BAO) observations. Additionally, we perform a complete dynamical system analysis in order to extract information of the local and global features of the cosmological evolution.

The outline of the paper is as follows: Section 2 introduces the framework of the Kaniadakis cosmology. In Section 3.1, we infer the cosmological parameter under the Kaniadakis model using five observational data sets mentioned above. Section 4 presents a stability analysis around the equilibrium points of the dynamical system under the Kaniadakis cosmology. Finally, we discuss and summarize our results in Section 5. From now on, we use natural units in which $\hbar = k_B = c = 1$.

2 KANIADAKIS HORIZON-ENTROPY COSMOLOGY

In this section, we present the scenario of Kaniadakis horizon-entropy cosmology (Lymperis et al. 2021), namely the modified Friedmann equations arising from the application of the gravity-thermodynamics conjecture using the extended Kaniadakis entropy.

Kaniadakis entropy is a one-parameter generalization of the classical entropy, given as $S_K = -k_B \sum_i n_i \ln_{\{K\}} n_i$ (Kaniadakis 2002, 2005), with k_B the Boltzmann constant and where $\ln_{\{K\}} x = (x^K - x^{-K})/2K$. In such a framework, the dimensionless parameter $-1 < K < 1$ quantifies the relativistic deviations from standard statistical mechanics, and the latter is recovered in the limit $K \to 0$. Kaniadakis entropy can be expressed as (Abreu et al. 2016, 2018; Abreu & Ananias Neto 2021)

$$S_K = -k_B \sum_{i=1}^{W} \frac{P_i^{1+K} - P_i^{1-K}}{2K}, \tag{1}$$

with P_i the probability of a specific microstate and W the total configuration number. When we apply it in the black hole framework, we obtain (Moradpour, Ziaie & Kord Zangeneh 2020; Drepanou et al. 2021; Lymperis et al. 2021)

$$S_K = \frac{1}{K} \sinh(K S_{BH}), \tag{2}$$

where

$$S_{BH} = \frac{1}{4G} A, \tag{3}$$

is the usual Bekenstein–Hawking entropy, with A the horizon area and G the gravitational constant. Hence, in the limit $K \to 0$, we recover Bekenstein–Hawking entropy.

Let us now apply the gravity-thermodynamics conjecture using Kaniadakis entropy. We consider a flat homogeneous and isotropic Friedmann–Robertson–Walker metric of the form

$$ds^2 = -dt^2 + a^2(t) \left(dr^2 + r^2 d\Omega^2 \right), \tag{4}$$

where $d\Omega^2 \equiv d\theta^2 + \sin^2\theta d\varphi^2$ is the solid angle, and $a(t)$ the scale factor. In this setup, the first law of thermodynamics is interpreted in terms of the heat/energy that flows through the apparent horizon of the Universe (Jacobson 1995; Padmanabhan 2005, 2010), which in the case of flat geometry is just (Bak & Rey 2000; Frolov & Kofman 2003; Cai & Kim 2005; Cai, Cao & Hu 2009)

$$r_a = \frac{1}{H}, \tag{5}$$

where $H = \dot{a}/a$ is the Hubble parameter (dots denote derivatives with respect to t). Concerning the horizon temperature, this is given by the standard relation (Gibbons & Hawking 1977):

$$T = \frac{1}{2\pi r_a}. \tag{6}$$

Hence, the first law of thermodynamics is just $-dE = TdS$, where $-dE = A(\rho_m + p_m)Hr_a dt$ is the energy flow through the horizon during a time interval dt in the case of a Universe filled with a matter perfect fluid with energy density ρ_m and pressure p_m (Cai & Kim 2005). Differentiating equation (2), we obtain

$$dS_K = \frac{8\pi}{4G} \cosh\left(K \frac{\pi}{GH^2} \right) r_a \dot{r}_a dt, \tag{7}$$

where we have used that $A = 4\pi r_a^2 = 4\pi/H^2$.

Inserting equations (3), (6), and (7) into the first law of thermodynamics, alongside with the relation $\dot{r}_a = -\dot{H}/H^2$, we acquire

(Lymperis et al. 2021)

$$-4\pi G(\rho_m + p_m) = \dot{H} \cosh\left[K\frac{\pi}{GH^2}\right]. \tag{8}$$

Thus, using the matter conservation equation

$$\dot{\rho}_m + 3H(\rho_m + p_m) = 0, \tag{9}$$

the integration of equation (8) leads to

$$\frac{8\pi G}{3}\rho_m = H^2 \cosh\left[K\frac{\pi}{GH^2}\right] - \frac{K\pi}{G}\text{shi}\left[K\frac{\pi}{GH^2}\right] - \frac{\Lambda}{3}, \tag{10}$$

with Λ the integration constant and $\text{shi}(x) \equiv \int_0^x \sinh(x')/x' dx'$, a mathematical odd function of x with no discontinuities.

Equations (8) and (10) are the modified Friedmann equations in the scenario of Kaniadakis horizon-entropy cosmology (Lymperis et al. 2021). As expected, in the limit $K \to 0$, they turn into the standard ones. We can rewrite them as

$$H^2 = \frac{8\pi G}{3}(\rho_m + \rho_{DE}), \tag{11}$$

$$\dot{H} = -4\pi G(\rho_m + \rho_{DE} + p_m + p_{DE}), \tag{12}$$

where we have introduced an effective dark energy sector, with energy density and pressure, respectively, of the form

$$\rho_{DE} = \frac{3}{8\pi G}\left\{\frac{\Lambda}{3} + H^2\left[1 - \cosh\left(\frac{\pi K}{GH^2}\right)\right] + \frac{\pi K}{G}\text{shi}\left(\frac{\pi K}{GH^2}\right)\right\}, \tag{13}$$

$$p_{DE} = -\frac{1}{8\pi G}\left\{\Lambda + (3H^2 + 2\dot{H})\left[1 - \cosh\left(\frac{\pi K}{GH^2}\right)\right] + \frac{3\pi K}{G}\text{shi}\left(\frac{\pi K}{GH^2}\right)\right\}. \tag{14}$$

Therefore, the EoS parameter for the dark energy sector is

$$w_{DE} = -1 - 2\dot{H}\left[1 - \cosh\left(\frac{\pi K}{GH^2}\right)\right]$$
$$\times \left\{\Lambda + 3H^2\left[1 - \cosh\left(\frac{\pi K}{GH^2}\right) + \frac{3\pi K}{G}\text{shi}\left(\frac{\pi K}{GH^2}\right)\right]\right\}^{-1}. \tag{15}$$

In the general case, the cosmological equations are the two Friedmann equations (11) and (12), alongside the matter conservation equation (9). *For convenience, we focus on on the dust case, namely we consider $p_m = 0$.* It proves convenient to express the equations in terms of dimensionless variables. Introducing the density parameters

$$\Omega_\Lambda \equiv \frac{\Lambda}{3H^2}, \quad \Omega_m \equiv \frac{8\pi G\rho_m}{3H^2}, \tag{16}$$

the normalized Hubble function

$$E \equiv \frac{H}{H_0}, \tag{17}$$

with H_0 the Hubble parameter at the present scale factor a_0, and defining the dimensionless parameter β as

$$\beta \equiv \frac{K\pi}{GH_0^2}, \tag{18}$$

then, the cosmological equations are expressed as

$$\Omega'_\Lambda(N) = 3\Omega_\Lambda\Omega_m\text{sech}\left(\frac{\beta}{E^2}\right), \tag{19}$$

$$\Omega'_m(N) = 3\Omega_m\left[\Omega_m\text{sech}\left(\frac{\beta}{E^2}\right) - 1\right], \tag{20}$$

$$E'(N) = -\frac{3}{2}E\Omega_m\text{sech}\left(\frac{\beta}{E^2}\right), \tag{21}$$

where primes denote derivatives with respect to the e-foldings number $N = \ln(a/a_0)$ (and thus $f' = \dot{f}/H$). Note that using the above variables, the first Friedmann equation (11) gives rise to the constraint

$$\beta\text{shi}\left(\frac{\beta}{E^2}\right) + E^2\left[-\cosh\left(\frac{\beta}{E^2}\right) + \Omega_\Lambda + \Omega_m\right] = 0, \tag{22}$$

which allows us to eliminate Ω_Λ in terms of Ω_m and E. Finally, note that for the effective dark energy density parameter, in the general case, we have

$$\Omega_{DE} = 1 - \Omega_m = 1 + \beta\text{shi}(\beta) - \cosh(\beta) + \Omega_\Lambda. \tag{23}$$

Lastly, it proves convenient to introduce the deceleration parameter $q(z)$, and the cosmographic jerk parameter $j(z)$, which are defined as

$$q := -1 - \frac{E'}{E}, \tag{24}$$

$$j := q(2q + 1) - q', \tag{25}$$

where $j = 1$ recovers the case of a CC.

In the scenario of Kaniadakis horizon-entropy cosmology, one may have the general integration constant Λ, which will play the role of an explicit CC, or one may set it to zero and thus require for the extra K-dependent terms to drive the Universe acceleration. Since the corresponding equation structure (which will be used later for the Bayesian statistical analysis and the dynamical system approach) is different in the two cases, we examine them separately in the following subsections.

2.1 Case I: $\Lambda \neq 0$

In the general case where $\Lambda \neq 0$, i.e. $\Omega_\Lambda \neq 0$, we use the constraint equation (22) to obtain the reduced dynamical system

$$\Omega'_m(N) = 3\Omega_m\left[\Omega_m\text{sech}\left(\frac{\beta}{E^2}\right) - 1\right], \tag{26}$$

$$E'(N) = -\frac{3}{2}E\Omega_m\text{sech}\left(\frac{\beta}{E^2}\right). \tag{27}$$

This is integrable, with

$$\Omega_m(E) = \cosh\left(\frac{\beta}{E^2}\right) + \frac{-\cosh(\beta) - \beta\text{shi}\left(\frac{\beta}{E^2}\right) + \beta\text{shi}(\beta) + \Omega_m^{(0)}}{E^2}, \tag{28}$$

$$\Omega_m(1) = \Omega_m^{(0)}, \tag{29}$$

and

$$E'(N) = -\frac{3}{2}E - \frac{3\text{sech}\left(\frac{\beta}{E^2}\right)\left(-\cosh(\beta) - \beta\text{shi}\left(\frac{\beta}{E^2}\right) + \beta\text{shi}(\beta) + \Omega_m^{(0)}\right)}{2E}, \tag{30}$$

where $\Omega_m(N = 0) = \Omega_m^{(0)}$ and $E(N = 0) = 1$.

Equation (30) is easily integrated to give

$$3N(E) = -\ln\left(1 - \frac{\cosh(\beta) - E^2\cosh\left(\frac{\beta}{E^2}\right) + \beta\text{shi}\left(\frac{\beta}{E^2}\right) - \beta\text{shi}(\beta)}{\Omega_m^{(0)}}\right), \tag{31}$$

introducing as a dynamical variable the redshift $e^N = a = (1 + z)^{-1}$, where $z = 0$ and $a_0 = 1$ for current time, and the previous

equation leads to

$$(z+1)^3 = 1 - \frac{\left[\cosh(\beta) - E^2 \cosh\left(\frac{\beta}{E^2}\right) + \beta \mathrm{shi}\left(\frac{\beta}{E^2}\right) - \beta \mathrm{shi}(\beta)\right]}{\Omega_{\mathrm{m}}^{(0)}}.$$
(32)

Evaluating equation (23) at present time gives

$$\Omega_{\mathrm{DE}}^{(0)} = 1 - \Omega_{\mathrm{m}}^{(0)} = 1 + \beta \mathrm{shi}(\beta) - \cosh(\beta) + \Omega_{\Lambda}^{(0)},$$
(33)

and combining it with equation (32) we have

$$\Omega_{\mathrm{m}}^{(0)}(z+1)^3 + \Omega_{\Lambda}^{(0)} = E^2 \cosh\left(\frac{\beta}{E^2}\right) - \beta \mathrm{shi}\left(\frac{\beta}{E^2}\right).$$
(34)

We mention here that in the general case where $\Lambda \neq 0$ from the above, we obtain the relation between β, $\Omega_{\mathrm{m}}^{(0)}$, and $\Omega_{\Lambda}^{(0)}$ as

$$\Omega_{\mathrm{m}}^{(0)} = \cosh(\beta) - \beta \mathrm{shi}(\beta) - \Omega_{\Lambda}^{(0)}.$$
(35)

We expand equations (33) and (34) up to third order around $\beta = 0$, resulting in

$$\Omega_{\mathrm{m}}^{(0)} + \Omega_{\Lambda}^{(0)} = 1 - \frac{\beta^2}{2} + O\left(\beta^4\right),$$
(36)

and

$$\Omega_{\mathrm{m}}^{(0)}(z+1)^3 + \Omega_{\Lambda}^{(0)} \approx E^2 - \frac{\beta^2}{2E^2} + O\left(\beta^4\right).$$
(37)

Hence, we obtain four roots:

$$E_{1,2} = \mp \frac{\sqrt{\Omega_{\mathrm{m}}^{(0)}(z+1)^3 + \Omega_{\Lambda}^{(0)} - \sqrt{2\beta^2 + \left[\Omega_{\mathrm{m}}^{(0)}(z+1)^3 + \Omega_{\Lambda}^{(0)}\right]^2}}}{\sqrt{2}},$$
(38)

$$E_{3,4} = \mp \frac{\sqrt{\Omega_{\mathrm{m}}^{(0)}(z+1)^3 + \Omega_{\Lambda}^{(0)} + \sqrt{2\beta^2 + \left[\Omega_{\mathrm{m}}^{(0)}(z+1)^3 + \Omega_{\Lambda}^{(0)}\right]^2}}}{\sqrt{2}}.$$
(39)

Solutions E_1 and E_2 are complex, and E_3 is negative. Thus, the only physical solution is E_4. In the following, instead of using the exact implicit formula for E given in equation (34), we will consider the approximation E_4 in equation (39).

2.2 Case II: $\Lambda = 0$

In the case where an explicit CC is absent, namely $\Lambda = 0$, i.e. $\Omega_{\Lambda} = 0$, the general system (26) and (27) reduces to

$$E'(N) = -\frac{3}{2}E + \frac{3\beta \mathrm{sech}\left(\frac{\beta}{E^2}\right)\mathrm{shi}\left(\frac{\beta}{E^2}\right)}{2E}.$$
(40)

The last equation is easily integrated to give

$$N(E) = -\frac{1}{3}\ln\left[\frac{E^2 \cosh\left(\frac{\beta}{E^2}\right) - \beta \mathrm{shi}\left(\frac{\beta}{E^2}\right)}{\cosh(\beta) - \beta \mathrm{shi}(\beta)}\right],$$
(41)

which, using the redshift, implies

$$(z+1)^3 = \frac{E^2 \cosh\left(\frac{\beta}{E^2}\right) - \beta \mathrm{shi}\left(\frac{\beta}{E^2}\right)}{\cosh(\beta) - \beta \mathrm{shi}(\beta)}.$$
(42)

Hence, using

$$\Omega_{\mathrm{m}}^{(0)} = \cosh(\beta) - \beta \mathrm{shi}(\beta),$$
(43)

as it arises from equation (35) for $\Omega_{\Lambda}^{(0)} = 0$, we obtain

$$\Omega_{\mathrm{m}}^{(0)}(z+1)^3 = E^2 \cosh\left(\frac{\beta}{E^2}\right) - \beta \mathrm{shi}\left(\frac{\beta}{E^2}\right).$$
(44)

Expanding equation (44) up to third order around $\beta = 0$ results in

$$\Omega_{\mathrm{m}}^{(0)}(z+1)^3 \approx E^2 - \frac{\beta^2}{2E^2} + O\left(\beta^4\right),$$
(45)

and thus at present times gives $\Omega_{\mathrm{m}}^{(0)} = 1 - \frac{\beta^2}{2} + O\left(\beta^4\right)$. Therefore, we obtain four roots:

$$E_{1,2} = \mp \frac{\sqrt{\Omega_{\mathrm{m}}^{(0)}(z+1)^3 - \sqrt{2\beta^2 + \Omega_{\mathrm{m}}^{(0)2}(z+1)^6}}}{\sqrt{2}},$$
(46)

$$E_{3,4} = \mp \frac{\sqrt{\Omega_{\mathrm{m}}^{(0)}(z+1)^3 + \sqrt{2\beta^2 + \Omega_{\mathrm{m}}^{(0)2}(z+1)^6}}}{\sqrt{2}}.$$
(47)

Similarly to the previous case, roots E_1 and E_2 are complex, while E_3 is negative. Consequently, the only physical solution is E_4 in equation (47).

3 OBSERVATIONAL CONSTRAINTS

In this section, we confront the scenario of Kaniadakis horizon-entropy cosmology with observations. We are interested in extracting the bounds on the parameter phase space $\Theta = \{h, \Omega_{\mathrm{m}}^{(0)}, \beta\}$ and $\{h, \beta\}$, particularly on the parameter β, which is related to the Kaniadakis basic parameter K. For convenience, we focus on the physically interested case of dust matter, namely we set $w_{\mathrm{m}} = 0$.

3.1 Data sets and methodology

We will employ the most commonly used data sets.

(i) *Observational Hubble data* (OHD). The sample contains 31 cosmological-independent measurements of the Hubble parameter in the redshift range $0.07 < z < 1.965$ from passive elliptic galaxies, the so-called cosmic chronometers (Moresco et al. 2016).

(ii) *Pantheon supernova Type Ia sample* (SNIa). We use 1048 data points of the distance modulus, $\mu(z)_{\mathrm{SNIa}}$, of high-redshift SNIa in the redshift range $0.001 < z < 2.3$ (Scolnic et al. 2018).

(iii) *H II galaxies* (HIIG). It contains a total of 181 data points of the distance modulus $\mu_{\mathrm{HIIG}}(z)$ estimated from the Balmer line luminosity–velocity dispersion relation for HIIG spanning the red-shift region $0.01 < z < 2.6$ (González-Morán et al. 2021).

(iv) *Strong lensing systems* (SLSs). We use the sample by Amante et al. (2020), which contains 143 SLSs by elliptical galaxies with measurements of the redshift for the lens and the source, spectroscopic velocity dispersion, and the Einstein radius. These quantities allow us to construct an observational distance ratio within the region $0.5 \leq D^{\mathrm{obs}} \leq 1$.

(v) *Baryon acoustic oscillations* (BAO). We consider six correlated data points of the imprint of BAO in the size of the sound horizon in clustering and power spectrum of galaxies measured by Percival et al. (2010), Blake et al. (2011), and Beutler et al. (2011), and collected by Giostri et al. (2012).

We would like to mention here that other cosmological observations could be included in the parameter estimation too, for instance the CMB data. To perform such analysis in a robust way, a full perturbation approach is needed in order to obtain the linear Einstein–Boltzmann equations. Nevertheless, this is beyond the scope of this work. An alternative approach would be to use the distance priors from Planck 2018 based on slight deviations from ΛCDM, such as the wCDM model (Chen, Huang & Wang 2019). However, since this procedure could lead to biased constraints, in the following, we prefer not to use the CMB data set.

The inference of the cosmological parameters under Kaniadakis horizon-entropy cosmology for both scenarios ($\Lambda \neq 0$ and $\Lambda = 0$) is performed by a Bayesian Markov chain Monte Carlo (MCMC) approach and the EMCEE PYTHON module (Foreman-Mackey et al. 2013). We set 3000 chains with 250 steps each, and consider uniform priors in the ranges: h: [0.2, 1], $\Omega_m^{(0)}$: [0, 1], and β: $[-\pi, \pi]$. The burn-in phase is stopped up to obtain convergence according to the autocorrelation time criterion. Then, we build a Gaussian log-likelihood as the figure-of-merit function to minimize through the equation $-2 \ln(\mathcal{L})\chi^2$, where χ is the chi-square function given by

$$\chi_{\text{uncorr}}^2 = \sum_i^{N_{\text{dat}}} \left(\frac{\mathcal{D} - \mathcal{M}}{\sigma_{\mathcal{D}}} \right)^2, \tag{48}$$

for the samples OHD, HIIG, and SLS because the measurements are considered to be uncorrelated. N_{dat} is the number of points of data set $\mathcal{D}$, $\sigma_{\mathcal{D}}$ is the estimated uncertainty for each data set, and $\mathcal{M}$ represents the theoretical quantity of that observable *based on E_4 presented in equations (39) and (47) for $\Lambda \neq 0$ and $\Lambda = 0$ models, respectively.* As SNIa and BAO data sets contain correlated points, the figure of merit is built as

$$\chi_{\text{corr}}^2 = \Delta \boldsymbol{x} \cdot \mathbf{C}^{-1} \cdot \Delta \boldsymbol{x}^T, \tag{49}$$

where $\Delta \boldsymbol{x}$ is the difference between the observational and theoretical quantities, and $\mathbf{C}^{-1}$ is the covariance matrix. It is worth mentioning that a nuisance parameter is presented in the SNIa data, and it is convenient to marginalize over it to reduce the uncertainties. Thus, the figure of merit for SNIa data is

$$\chi_{\text{SNIa}}^2 = a + \ln \left(\frac{e}{2\pi} \right) - \frac{b^2}{e}, \tag{50}$$

where a, b, and e are functions of $\Delta \boldsymbol{x}$ and $\mathbf{C}^{-1}$. For more details on these expressions, see Motta et al. (2021).

Finally, we perform a joint analysis through the sum of the function-of-merits of each data sample, namely

$$\chi_{\text{Joint}}^2 = \chi_{\text{OHD}}^2 + \chi_{\text{SLS}}^2 + \chi_{\text{HIIG}}^2 + \chi_{\text{SNIa}}^2 + \chi_{\text{BAO}}^2, \tag{51}$$

where subscripts indicate the data set under consideration.

3.2 Results

Performing the full confrontation of the scenario, we construct the corresponding log-likelihood contours at 68 per cent (1σ) and 99.7 per cent (3σ) confidence level (CL), and we present them in Fig. 1 alongside the one-dimensional (1D) posterior distribution. Moreover, in Table 1, we show the mean values and the uncertainties at 1σ CL for the parameters h, $\Omega_m^{(0)}$, and β for both $\Lambda \neq 0$ and $\Lambda = 0$ cases.

As can be seen, the bounds estimated from each data sample are consistent among themselves, although the SLS data set provides lower values for $\Omega_m^{(0)}$. The joint constraints $h = 0.708_{-0.011}^{+0.012}$ ($h = 0.715_{-0.012}^{+0.012}$) for the case $\Lambda \neq 0$ ($\Lambda = 0$) are consistent at 2.67σ (3σ) with the one estimated from the CMB anisotropies (Aghanim et al. 2020) and at 1.74σ (1.36σ) with the one from SH0ES (Riess et al. 2019). Hence, the scenario of Kaniadakis horizon-entropy cosmology can offer an alleviation to the H_0 tension, providing a value in between its local measurements and its indirect estimation from the early stages of the Universe.

Concerning the Kaniadakis parameter, we find that, when $\Lambda \neq 0$, the combination of the data samples constrains $\beta = -0.011_{-0.507}^{+0.515}$, namely β is constrained around 0 as expected, the value in which Kaniadakis entropy becomes the standard Bekenstein–Hawking one.

However, when $\Lambda = 0$, the joint constraint yields $\beta = 1.161_{-0.013}^{+0.013}$, which is expected, as we mentioned above, because in the absence of an explicit CC, one needs a significant deviation from standard cosmology to describe the Universe acceleration. Finally, note that due to equation (43) that holds in the $\Lambda = 0$ case, we acquire a correlation between $\Omega_m^{(0)}$ and the Kaniadakis parameter β in the lower panel of Fig. 1.

Let us make a comment on the predicted entropy today, since this is possible to be calculated through equation (2). According to our model, and imposing for the horizon area of our Universe its present value, we arrive at the values $S_K \sim 1.44 \times 10^{99}$ m^2 kg s^{-2} K^{-1} (for $\Lambda \neq 0$) and $S_K \sim 3.15 \times 10^{99}$ m^2 kg s^{-2} K^{-1} (for $\Lambda = 0$). In comparison, for the standard Bekenstein–Hawking entropy, we have $S_{BH} \sim 2.83 \times 10^{99}$ m^2 kg s^{-2} K^{-1} ($\Lambda \neq 0$) and $S_{BH} \sim 2.79 \times 10^{99}$ m^2 kg s^{-2} K^{-1} ($\Lambda = 0$). Therefore, the corresponding ratio is $S_K/S_{BH} \simeq 0.5$ for $\Lambda \neq 0$ and $S_K/S_{BH} \simeq 1.12$ for $\Lambda = 0$, which implies a small difference between Kaniadakis and Bekenstein–Hawking entropies.

Due to the competitive qualities of the fits obtained from both scenarios, it would be interesting to statistically compare them with the concordance ΛCDM cosmology. In order to achieve this, we apply the standard criteria, namely the Akaike information criterion corrected for small samples (AICc; Akaike 1974; Sugiura 1978; Hurvich & Tsai 1989) and the Bayesian information criterion (BIC; Schwarz 1978), since the $\Lambda \neq 0$ model contains one extra free parameter over ΛCDM. The AICc and BIC are defined as AICc = $\chi_{\min}^2 + 2k + (2k^2 + 2k)/(N - k - 1)$ and BIC = $\chi_{\min}^2 + k \ln(N)$, respectively, where $\chi_{\min}^2$ is the minimum of the χ^2 function, N is the size of the data set, and k is the number of free parameters. Following the rules described in Hernández-Almada et al. (2022), we find that $\Lambda = 0$ model and ΛCDM are statistically equivalent based on AICc (ΔAICc < 4), when the samples are treated separately, but show strong evidence against ($6 < \text{BIC} < 10$) the scenario when the joint analysis is applied. On the other hand, although AICc suggests that $\Lambda \neq 0$ model and ΛCDM are statistically equivalent in the joint analysis, BIC indicates that there is strong evidence against the candidate model. Additionally, for the two models, we find that the $\Lambda = 0$ case is preferred by separate data sets, while the $\Lambda \neq 0$ case is statistically preferred for the combined data analysis.

For completeness, we additionally calculate the deviance information criterion (DIC; Spiegelhalter et al. 2002; Kunz, Trotta & Parkinson 2006; Liddle 2007). This is defined as DIC = $D(\bar{\theta}) + 2p_D$, where $D(\bar{\theta}) = \chi^2(\bar{\theta})$ is the Bayesian deviation, $p_D = \bar{D}(\theta) - D(\bar{\theta})$ is the Bayesian complexity, which represents the number of effective degrees of freedom, and $\bar{\theta}$ is the mean value of the parameters. The advantage of DIC is its use of the full log-likelihood sample instead of only the maximum log-likelihood (or minimum χ^2) as AICc and BIC do. Based on the Jeffreys scale (Jeffreys 1961), for ΔDIC < 2, both models are statistical equivalent. In contrast, $2 < \Delta$DIC < 6 suggests a moderate tension between models, being the one with lower value of DIC the best one, and ΔDIC > 10 implies a strong tension between the two models. We find that the $\Lambda \neq 0$ case and ΛCDM scenario are statistical equivalent for BAO, they have a moderate tension for OHD and SLS, and a strong tension for HIIG and SNIa. On the other hand, the $\Lambda \neq 0$ case and ΛCDM are statistical equivalent for OHD, BAO, HIIG, and SNIa. In summary, we confirm the results obtained for the joint analysis by AICc and BIC for both $\Lambda \neq 0$ and $\Lambda = 0$ models. It is worth mentioning that when a posterior distribution presents a bimodal shape or is asymmetric for a parameter, p_D yields negative values and thus DIC may not be a good criterion. This situation is mainly presented for β in the $\Lambda \neq 0$ case in separate data sets.
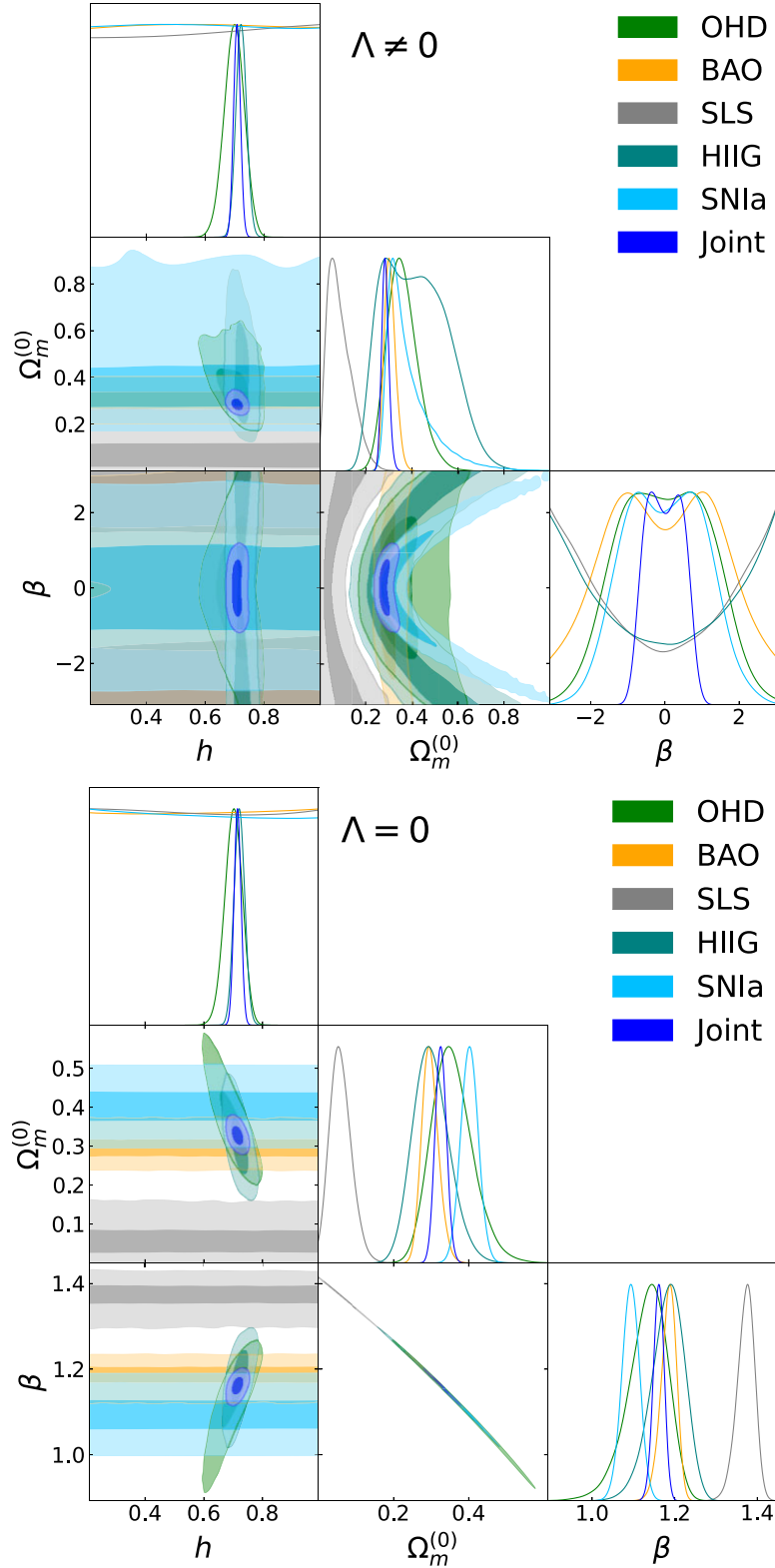
Figure 1. 2D log-likelihood contours at 68 per cent and 99.7 per cent CL, alongside the corresponding 1D posterior distribution of the free parameters, in Kaniadakis horizon-entropy cosmology, for $\Lambda \neq 0$ (upper panel) and $\Lambda = 0$ (lower panel). We use the various data sets described in the text, as well as the joint analysis.

As a next step, we use the constraints from the joint analysis to reconstruct the three cosmographic parameters, namely the Hubble, $H(z)$, the deceleration, $q(z)$, and jerk, $j(z)$, parameters according to equations (24) and (25). The cosmic evolution of parameters is shown in Fig. 2. Thus, we report the current values of $q_0 = -0.610^{+0.028}_{-0.035}$ $(-0.708^{+0.016}_{-0.016})$ for the deceleration parameter, and $j_0 = 1.041^{+0.051}_{-0.036}$ $(1.137^{+0.014}_{-0.013})$ for the jerk parameter for the $\Lambda \neq 0$ ($\Lambda = 0$) scenario. Furthermore, the transition redshift between the deceleration and the

Table 1. Best-fitting values and their 68 per cent CL uncertainties for Kaniadakis horizon-entropy cosmology with $\Lambda \neq 0$ (upper panel) and $\Lambda = 0$ (lower panel) employing the data sets: OHD (31 data points), BAO (6 data points), SLS (143 data points), HIIG (181 data points), SNIa (1048 data points), and the joint analysis of them.

Sample	$\chi^2_{\min}$	h	$\Omega_m^{(0)}$	β	ΔAICc	ΔBIC	ΔDIC
			Case $\Lambda \neq 0$				
OHD	19.25	$0.699^{+0.033}_{-0.034}$	$0.354^{+0.072}_{-0.061}$	$-0.004^{+1.259}_{-1.255}$	7.6	8.2	-4.5
BAO	2.91	$0.599^{+0.272}_{-0.270}$	$0.302^{+0.027}_{-0.023}$	$-0.016^{+1.596}_{-1.594}$	14.1	1.9	0.2
SLS	216.52	$0.608^{+0.268}_{-0.277}$	$0.077^{+0.064}_{-0.042}$	$-0.006^{+2.550}_{-2.526}$	5.5	8.3	-5.2
HIIG	452.96	$0.722^{+0.018}_{-0.018}$	$0.408^{+0.151}_{-0.137}$	$0.043^{+2.510}_{-2.562}$	19.3	22.3	-19.6
SNIa	1042.99	$0.598^{+0.273}_{-0.270}$	$0.359^{+0.126}_{-0.055}$	$0.009^{+1.108}_{-1.124}$	9.0	14.0	-14.6
Joint	1743.48	$0.708^{+0.012}_{-0.011}$	$0.283^{+0.016}_{-0.015}$	$-0.011^{+0.517}_{-0.507}$	2.9	8.1	0.5
			Case $\Lambda = 0$				
OHD	14.56	$0.701^{+0.029}_{-0.030}$	$0.353^{+0.057}_{-0.050}$	$1.138^{+0.043}_{-0.051}$	0.5	0.0	0.0
BAO	2.33	$0.602^{+0.272}_{-0.273}$	$0.297^{+0.023}_{-0.021}$	$1.186^{+0.017}_{-0.020}$	3.6	-0.4	-0.3
SLS	212.86	$0.596^{+0.276}_{-0.270}$	$0.057^{+0.031}_{-0.027}$	$1.373^{+0.020}_{-0.023}$	-0.2	-0.3	0.0
HIIG	435.64	$0.721^{+0.018}_{-0.018}$	$0.298^{+0.050}_{-0.045}$	$1.185^{+0.038}_{-0.043}$	-0.1	-0.2	-0.1
SNIa	1036.48	$0.596^{+0.275}_{-0.271}$	$0.402^{+0.023}_{-0.023}$	$1.093^{+0.021}_{-0.021}$	0.5	0.5	0.5
Joint	1753.03	$0.715^{+0.012}_{-0.012}$	$0.326^{+0.015}_{-0.015}$	$1.161^{+0.013}_{-0.013}$	10.4	10.4	10.4
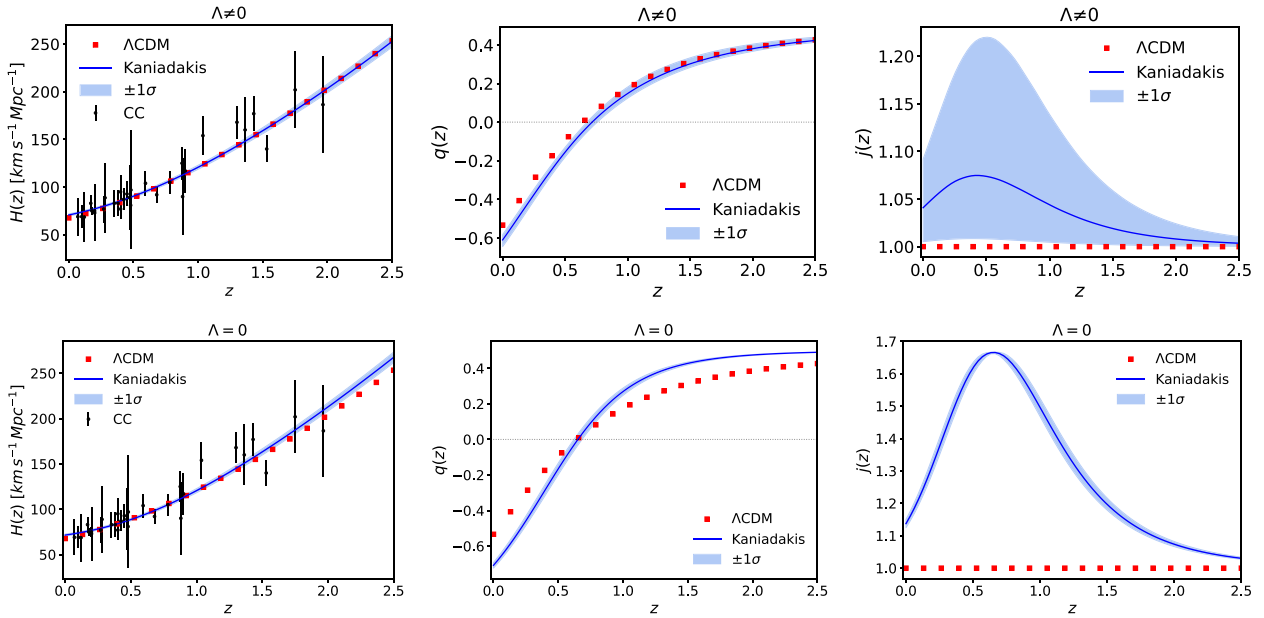
Figure 2. Upper panel, left to right: reconstruction of the $H(z)$, $q(z)$, and $j(z)$, in Kaniadakis horizon-entropy cosmology with $\Lambda \neq 0$. Lower panel: same as before for the case $\Lambda = 0$. We have used the bound obtained from the joint analysis, and the shaded regions denote the uncertainties at 1σ. For completeness, the red square points represent the results of ΛCDM cosmology with $h = 0.6766$ and $\Omega_m^{(0)} = 0.3111$ (Aghanim et al. 2020).

acceleration stages is estimated to be $z_T = 0.715^{+0.042}_{-0.041}$ ($0.652^{+0.032}_{-0.031}$), which is in agreement with the one obtained by ΛCDM as shown in Fig. 2. Note that the jerk parameter evolution reveals the dynamical EoS of the effective dark energy.

Finally, to investigate in more detail the Hubble tension, we apply a new diagnostic, called $\mathbb{H}0(z)$ diagnostic, defined by (Krishnan et al. 2021)

$$\mathbb{H}0(z) = \frac{H(z)}{E_{\Lambda CDM}(z)}, \qquad (52)$$

where $H(z)$ is the Hubble function evolution in a given cosmological scenario alternative to ΛCDM, and $E_{\Lambda CDM}(z)$ is the dimensionless Hubble parameter of ΛCDM paradigm. This diagnostic measures a

possible deviation of H_0 from its ΛCDM value. Concerning a flat ΛCDM, a non-constant path of $\mathbb{H}0(z)$ within error bars suggests a modification of the Planck-ΛCDM scenario. In Fig. 3, we depict the obtained results.

As we observe, there is an agreement within 1σ between flat-ΛCDM cosmology and Kaniadakis cosmology for $z \gtrsim 0.7$ in the $\Lambda \neq 0$ case, and for $0.7 \lesssim z \lesssim 1.3$ in the $\Lambda = 0$ case. Additionally, it is interesting that the current value $\mathbb{H}0(z=0)$ for both models is consistent with the one obtained by SH0ES (Riess et al. 2019), and that the $\Lambda \neq 0$ model has a trend to the Planck value in the past (Aghanim et al. 2020). This is another verification that the scenario of Kaniadakis horizon-entropy cosmology may offer an alleviation to the H_0 tension. Nevertheless, to further investigate whether both
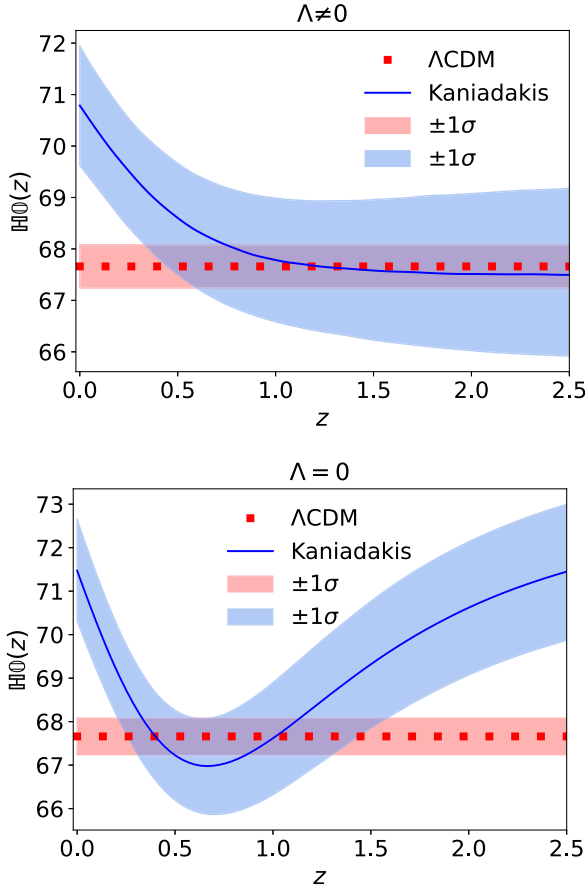
Figure 3. The $\mathbb{H}0(z)$ diagnostic for Kaniadakis horizon-entropy cosmology with $\Lambda \neq 0$ (upper panel) and $\Lambda = 0$ (lower panel). We have used the bound obtained from the joint analysis, and the shaded regions denote the uncertainties at 1σ. For completeness, the red square points represent the results of ΛCDM cosmology with $h = 0.6766$ and $\Omega_m^{(0)} = 0.3111$ (Aghanim et al. 2020).

Kaniadakis models can alleviate the Hubble tension, a parameter estimation using the linear perturbation equations together with CMB data should be performed.

We close this section by investigating one important process in every cosmological scenario: the big bang nucleosynthesis (BBN), since the production of light elements in the early Universe can be affected in non-standard cosmologies (Pospelov & Pradler 2010; Barrow, Basilakos & Saridakis 2021). Considering that the freeze-out of the light elements occurs when the weak interaction rates are lower than $H(z)$, a simple test to guarantee that the BBN is not spoiled is to require that the deviation $\delta H(z)$ with respect to the standard Hubble expansion rate at the BBN epoch should be small. Although in the Friedmann equations mentioned above, we have not included a radiation component, this can be added and we can perform the analysis by expanding E_4 around $\beta = 0$ in equation (39) (resp. equation 47) and neglecting the fourth-order error terms, resulting in

$$E(z) = \begin{cases} \underbrace{\sqrt{\Omega_m^{(0)}(z+1)^3 + \Omega_\Lambda^{(0)}}}_{\text{value from} \Lambda\text{CDM}} + \underbrace{\frac{\beta^2}{4}\left[\Omega_m^{(0)}(z+1)^3 + \Omega_\Lambda^{(0)}\right]^{-3/2}}_{\text{correction}}, \Lambda \neq 0 \\ \underbrace{\sqrt{\Omega_m^{(0)}(z+1)^{3/2}}}_{\text{value from} \Lambda\text{CDM}} + \underbrace{\frac{\beta^2}{4}\left[\Omega_m^{(0)}\right]^{-3/2}(z+1)^{-1/2}}_{\text{correction}}, \Lambda = 0 \end{cases}.$$

(53)

Hence, we can study both Kaniadakis models ($\Lambda \neq 0$ and $\Lambda = 0$) at $z \sim 10^{10}$ (approximately BBN era). We find that for $\Lambda \neq 0$, the model is consistent with the BBN constraints, since the correction term at $z \sim 10^{10}$ is of the order of $\sim 10^{-49}$, dominating the standard cosmology and not producing significant effects on the formation of light elements. In the case $\Lambda = 0$, the correction is larger, and calculations at $z \sim 10^{10}$ are of the order of $\sim 10^{-5}$. However, such corrections are still subdominant, allowing the production of light elements. A further analysis could be performed following Capozziello, Lambiase & Saridakis (2017), Barrow et al. (2021), and Asimakis et al. (2021).

4 DYNAMICAL SYSTEM AND STABILITY ANALYSIS

In this section, we perform a full dynamical system analysis in order to investigate the global dynamics of cosmological scenarios, and obtain information on the Universe evolution independently of the initial conditions. In the dynamical system formulation, one starts from a local analysis of the differential equation $x'(\tau) = X(x)$, where x is the state vector, and τ a convenient time variable, near an equilibrium point $x = \bar{x}$, and progressively extends the investigated regions of the phase and of the parameter space. Assuming that the vector field $X(x)$ has continuous partial derivatives, the process of determining the local behaviour is based on the linear approximation of the vector field $X(x) \approx DX(\bar{x})(x - \bar{x})$ where $DX(\bar{x})$ is the Jacobian of the vector field at the equilibrium point $\bar{x}$, which is referred to as the *linearization of the dynamical equations at the equilibrium point*. In this neighbourhood, we acquire the system $x'(\tau) = DX(\bar{x})(x - \bar{x})$. Each of the equilibrium points can be classified according to the real parts of the eigenvalues of $DX(\bar{x})$ (if none of these are zero). Thus, this approach provides a general description of the phase space of all possible solutions of the system, their equilibrium points and stability, as well as the asymptotic solutions (Ferreira & Joyce 1997; Wainwright & Ellis 1997; Copeland, Liddle & Wands 1998; Perko 2000; Coley 2003; Copeland, Sami & Tsujikawa 2006; Chen, Gong & Saridakis 2009; Giambo & Miritzis 2010; Cotsakis & Kittou 2013; Papagiannopoulos, Basilakos & Saridakis 2022). If some real parts of the eigenvalues are zero, the equilibrium point is non-hyperbolic, and the analysis through linearization fails. Then, we use numerical tools for the analysis.

In the following subsections, we perform the global dynamical system analysis for the two cases, namely $\Lambda \neq 0$ and $\Lambda = 0$.

4.1 Case I: $\Lambda \neq 0$

Defining the dimensionless variables θ, T as

$$\theta = \arctan\left(1 - \frac{8\pi G \rho_{\text{DE}}}{3H^2}\right), \theta \in \left[-\frac{\pi}{2}, \frac{\pi}{2}\right], \quad T = \frac{H_0}{H + H_0},$$

(54)

with

$$\Omega_m := \frac{8\pi G \rho_m}{3H^2} = \tan(\theta),$$

(55)

then equation (10) becomes

$$\frac{\Lambda}{3H_0^2} = \frac{(1-T)^2 \left\{\cosh\left[\frac{T^2 \beta}{(1-T)^2}\right] - \tan(\theta)\right\}}{T^2} - \beta \text{shi}\left[\frac{T^2 \beta}{(1-T)^2}\right].$$

(56)

Table 2. The equilibrium points of the dynamical system (58) and (59) of Kaniadakis horizon-entropy cosmology with $\Lambda \neq 0$. We use dS to denote the de Sitter, dark-energy-dominated solutions, and M to denote the matter-dominated ones.

Label	θ	T	Existence	Stability
dS_+	$2\pi c_1$	Arbitrary	$c_1 \in \mathbb{Z}$	Stable
$dS_+^{(0)}$	$2\pi c_1$	0	$c_1 \in \mathbb{Z}$	Stable
$dS_+^{(1)}$	$2\pi c_1$	1	$c_1 \in \mathbb{Z}$	Stable
dS_-	$\pi(1 + 2c_1)$	Arbitrary	$c_1 \in \mathbb{Z}$	Stable
$dS_-^{(0)}$	$\pi(1 + 2c_1)$	0	$c_1 \in \mathbb{Z}$	Stable
$dS_-^{(1)}$	$\pi(1 + 2c_1)$	1	$c_1 \in \mathbb{Z}$	Stable
$M_-^{(0)}$	$2\pi c_1 - \frac{3\pi}{4}$	0	$c_1 \in \mathbb{Z}$	Unstable
$M_+^{(0)}$	$2\pi c_1 + \frac{\pi}{4}$	0	$c_1 \in \mathbb{Z}$	Unstable
$M_-^{(1)}$	$2\pi c_1 - \frac{3\pi}{4}$	1	$c_1 \in \mathbb{Z}, \beta = 0$	Saddle
$M_+^{(1)}$	$2\pi c_1 + \frac{\pi}{4}$	1	$c_1 \in \mathbb{Z}, \beta = 0$	Saddle

It proves convenient to introduce the new time derivative as

$$f' \equiv \frac{df}{d\tau} = \frac{\cosh\left(\frac{\pi K}{GH^2}\right)}{H} \dot{f}. \tag{57}$$

Therefore, we finally extract the dynamical system

$$\theta'(\tau) = 3\sin(\theta)\left\{\sin(\theta) - \cos(\theta)\cosh\left[\frac{T^2\beta}{(1-T)^2}\right]\right\}, \tag{58}$$

$$T'(\tau) = \frac{3}{2}(1-T)T\tan(\theta). \tag{59}$$

Note that this system diverges at $T = 1$ and at $\theta = \pm\pi/2$.

Lastly, the deceleration parameter (24) is written as

$$q := -1 - \frac{\dot{H}}{H^2} = -1 + \frac{3}{2}\tan(\theta)\mathrm{sech}\left[\frac{\beta T^2}{(1-T)^2}\right]. \tag{60}$$

Note that, for an expanding universe ($H > 0$), we have $T \in [0, 1]$, while θ is a periodic coordinate with period π, and thus we can set $\theta \in [-\pi/2, \pi/2]$ (modulo a periodic shift $c\pi$, $c \in \mathbb{Z}$). Moreover, the physical condition $0 \leq \Omega_m \leq 1$ implies that the region of physical interest is $\theta \in [0, \pi/4]$ (modulo a periodic shift $c\pi$, $c \in \mathbb{Z}$). The non-physical region $\Omega_m > 1$ is $\theta \in (\pi/4, \pi/2]$ (modulo a periodic shift $c\pi$, $c \in \mathbb{Z}$). Hence, we have obtained a global phase-space formulation. For the representation of the flow of the system (58) and (59), we integrate in the variables T, θ and project in a compact set using the 'cylinder-adapted' coordinates

$$\boldsymbol{S} : \begin{cases} x = \cos(\theta), \\ y = \sin(\theta), \\ z = T, \end{cases} \tag{61}$$

with $0 \leq T \leq 1$, $\theta \in [-\pi, \pi]$, with inverse $\theta = \arctan(y/x)$, and $T = z$. Thus, the region of physical interest is $\theta \in [0, \pi/4]$, modulo a periodic shift $c\pi$, $c \in \mathbb{Z}$.

We proceed by extracting the equilibrium points and characterizing their stability. There are two equivalent hyperbolic equilibrium points $M_\pm$ for which $q = 1/2$, i.e. they are associated with matter domination, and two equilibrium points $dS_\pm$ corresponding to dark-energy-dominated de Sitter solutions for which $q = -1$. The equilibrium points of the dynamical system (58) and (59) of Kaniadakis horizon-entropy cosmology with $\Lambda \neq 0$ are presented in Table 2.

In Fig. 4, we display an unwrapped solution space of the system (58) and (59) (upper panel), and the projection over the cylinder $\boldsymbol{S}$, defined in Cartesian coordinates (x, y, z) by equation (61), for the best-fitting value $\beta = -0.011$ obtained through the observational analysis. For the points that are non-hyperbolic, their stability is analysed numerically. The two dashed lines, indicated by dS_- (blue)
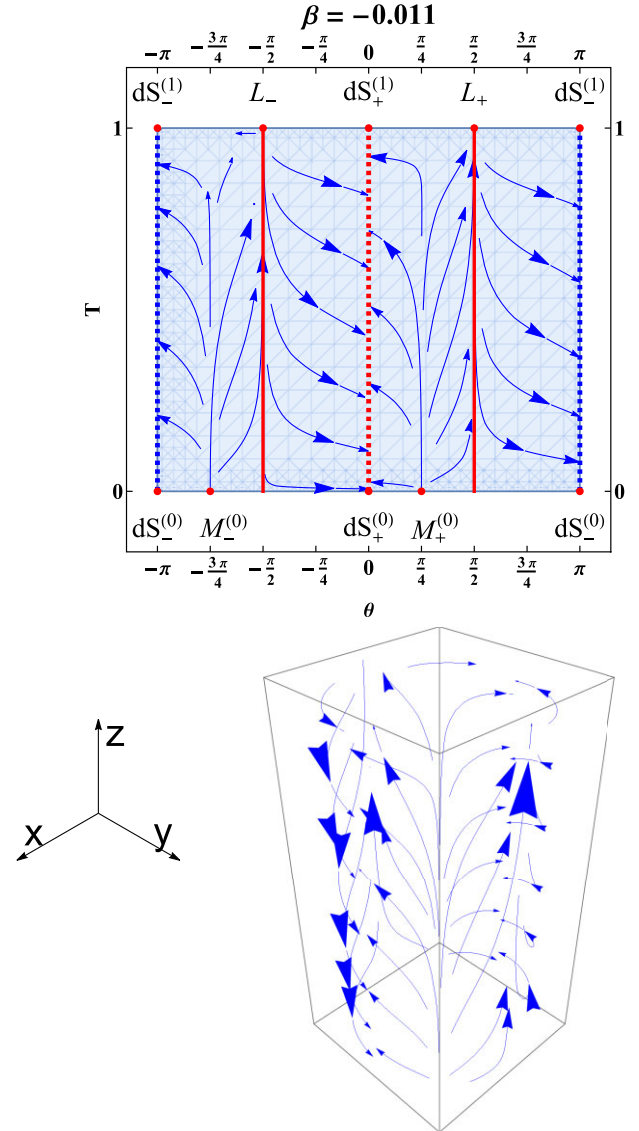

Figure 4. Phase-space plot of the dynamical system (58) and (59) of Kaniadakis horizon-entropy cosmology with $\Lambda \neq 0$, for the best-fitting value of Kaniadakis parameter obtained by the observational analysis, namely for $\beta = -0.011$. Upper panel: unwrapped solution space. Lower panel: projection over the cylinder $\boldsymbol{S}$ defined in Cartesian coordinates (x, y, z) through equation (61). At late times, the Universe results in a dark-energy-dominated, de Sitter solution, while the past attractor is the matter-dominated epoch.

and dS_+ (red), are the late-time de Sitter attractors. The early-time attractors are $M_\pm^{(0)}$ for which $q = 1/2$, and they correspond to matter-dominated solutions. Hence, at late times, the Universe results in a dark-energy-dominated solution, while the past attractor of the Universe is the matter-dominated epoch. At the intersection of the invariant set $T = 1$ with the singular lines $\theta = \pm\pi/2$, we obtain the equilibrium points $L_\pm$. Considering that equations (58) and (59) diverge at $L_\pm$, we should introduce suitable variables for the analysis.

For the analysis at $T = 1$, it proves convenient to define the variable

$$\Phi = \left\{1 + \exp\left[\frac{|\beta|T^2}{(1-T)^2}\right]\right\}^{-1}, \Phi \in [0, 1], \tag{62}$$
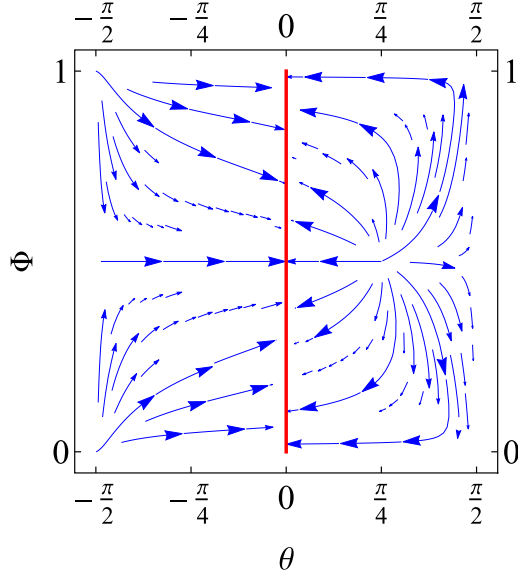
Figure 5. Phase-space plot of the system (64)–(65) of Kaniadakis horizon-entropy cosmology with $\Lambda \neq 0$, for dust matter. The late attractor corresponds to $\theta = 0$, and thus to a dark-energy-dominated solution with $\Omega_{DE} = 1$.

as well as the time rescaling

$$f' \equiv \frac{\mathrm{d}f}{\mathrm{d}\zeta} = (1 - \Phi)^2 \frac{\mathrm{d}f}{\mathrm{d}\eta} = \frac{\tanh^2\left(\frac{\pi|K|}{2GH^2}\right) + 1}{4H} \dot{f}. \quad (63)$$

Hence, using also the variable θ from equation (54), we finally obtain the autonomous system

$$\theta'(\zeta) = -\frac{3}{2} \sin(\theta) \left[2(\Phi - 1)\Phi(\sin(\theta) + \cos(\theta)) + \cos(\theta) \right], \quad (64)$$

$$\Phi'(\zeta) = 3(1 - \Phi)^2 \Phi^2 \tan(\theta) \ln \left[\Phi / (1 - \Phi) \right]. \quad (65)$$

In Fig. 5, we depict the phase-space flow of the system (64) and (65). Asymptotically, $\theta \to 0$ and Φ tends to a constant Φ_0. Therefore, the late attractor corresponds to the dark-energy-dominated solution with $\Omega_{DE} = 1$. The current values $\Phi_0 = 1/(e^{|\beta|} + 1)$, $\theta_0 = \arctan\left(\Omega_m^{(0)}\right)$ lead to the de Sitter solution $a(t) = e^{H_0(t - t_U)}$.

4.1.1 Heteroclinic sequences

In the phase portrait of a dynamical system, a heteroclinic orbit is a path in phase space that joins two different equilibrium points. If the equilibrium points at the start and end of the orbit are the same, the orbit is a homoclinic orbit (Guckenheimer & Holmes 1983).

From the above analysis, we can see that the invariant sets $T = 0$ and 1 are of interest in the determination of possible heteroclinic sequences. The direction of the flow can be determined by considering the monotonic function

$$M_1 = \frac{T}{1 - T}, \quad M_1'(\tau) = \frac{3\tan(\theta)}{2} M_1. \quad (66)$$

If $\tan(\theta) < 0$, the orbits move from $T = 1$ to 0, and if $\tan(\theta) > 0$, the orbits move from $T = 0$ to 1. In the invariant manifold $T = 0$ ($H \to \infty$), the dynamics is given by the 1D flow

$$\theta'(\tau) = 3 \sin(\theta) (\sin(\theta) - \cos(\theta)). \quad (67)$$

In Fig. 6, we present the 1D dynamical system (67), in which we can see the heteroclinic sequences $M_+^{(0)} \to dS_+^{(0)}$ and $M_-^{(0)} \to dS_-^{(0)}$.
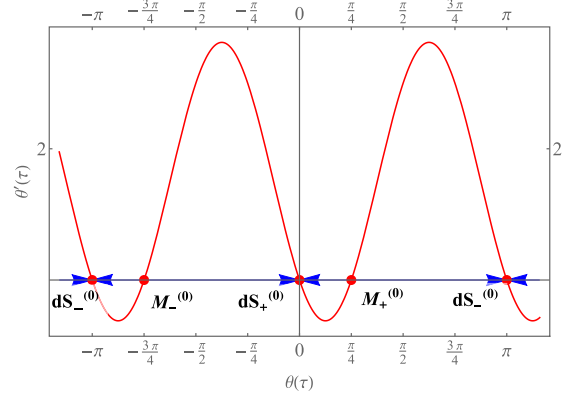
Figure 6. Phase-space diagram of the 1D dynamical system (67) of Kaniadakis horizon-entropy cosmology with $\Lambda \neq 0$, for dust matter and any value β.
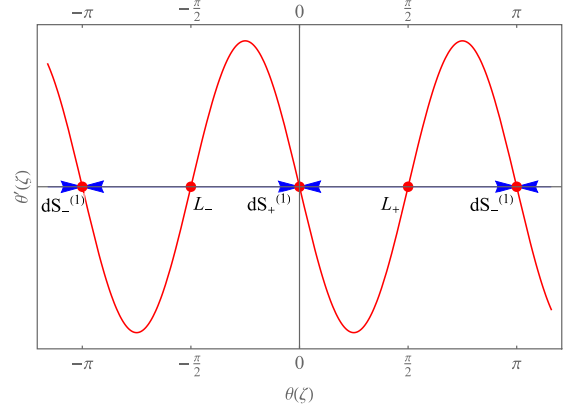
Figure 7. Phase-space diagram of the 1D dynamical system (68) of Kaniadakis horizon-entropy cosmology with $\Lambda \neq 0$, for dust matter and any value β.

Similarly, analysing the 1D flow in the invariant set $T = 1$, which corresponds to $\Phi = 0$, we find that the dynamics on this invariant set is given by the 1D dynamical system

$$\theta'(\zeta) = -\frac{3}{2} \sin(\theta) \cos(\theta), \quad (68)$$

which has a behaviour shown in Fig. 7, where the heteroclinic sequences $L_+ \to dS_+^{(1)}$ and $L_- \to dS_-^{(1)}$ are presented. Finally, to find heteroclinic sequences $M_\pm^{(0)} \to dS_\pm^{(1)}$, the intersection of the unstable manifold of $M_\pm^{(0)}$ with the stable manifold of $dS_\pm^{(1)}$ should be analysed. Since the former is $\mathbb{R}^2$, then it is required to examine the stable manifold of $dS_\pm^{(1)}$. This is given locally by the graph

$$\left\{ (\Phi, \theta) \in \mathbb{R}^2 : \Phi = h(\theta), h(0) = 0, h'(0) = 0 \right\}, |\theta| < \delta, \quad (69)$$

for $\delta > 0$ suitably small. By the invariance of the stable manifold, we obtain the quasi-linear differential equation for h given by

$$\frac{3}{2} \sin(\theta) h'(\theta)(2(h(\theta) - 1)h(\theta)(\sin(\theta) + \cos(\theta)) + \cos(\theta))$$

$$+ 3(h(\theta) - 1)^2 h(\theta)^2 \tan(\theta) \ln \left(\frac{h(\theta)}{1 - h(\theta)} \right) = 0. \quad (70)$$

Introducing the ansatz $h(\theta) = a_1 \theta^2 + a_2 \theta^3 + a_3 \theta^4 + \ldots$, we obtain $a_i = 0$ at any order. Therefore, the dynamics at the stable manifold of $dS_+^{(1)}$ is given by equation (68). Then, it is easy to construct heteroclinic sequences $M_+^{(0)} \to dS_+^{(1)}$, which pass near the singularity

L_+ by assuming, for instance, the initial value $(\Phi, \theta) = (\varepsilon, \pi/4)$, $\varepsilon \approx 0$ and evolving the system back and forward in ζ. Similar arguments can be used to construct heteroclinic sequences $M^{(0)}_- \to dS^{(1)}_-$, which pass near the singularity L_-, with the initial value $(\Phi, \theta) = (\varepsilon, -3\pi/4)$, $\varepsilon \approx 0$.

Summarizing, for $0 \leq \theta \leq \pi/2$ (the physical region is $0 \leq \theta \leq \pi/4$), there exist the heteroclinic sequences $M^{(0)}_+(\Omega_m \to 1, H \to \infty) \to L_+(\Omega_m \to +\infty, H \to 0) \to dS^{(1)}_+$(de Sitter, $\Omega_m \to 0$, $H \to 0$) and $M^{(0)}_+ \to dS^{(0)}_+$(de Sitter, $\Omega_m \to 0$, $H \to \infty$), and in the region $-\pi \leq \theta \leq -\pi/2$ (the physical region is $-\pi \leq \theta \leq -3\pi/4$), there exist the heteroclinic sequences $M^{(0)}_-(\Omega_m \to 1, H \to \infty) \to L_-(\Omega_m \to -\infty, H \to 0) \to dS^{(1)}_-$(de Sitter, $\Omega_m \to 0$, $H \to 0$) and $M^{(0)}_- \to dS^{(0)}_-$(de Sitter, $\Omega_m \to 0$, $H \to \infty$).

4.1.2 Bounce and a turnaround

Another interesting cosmological possibility is the possible existence of a bounce and a turnaround (Saridakis 2009; Cai, Gao & Saridakis 2012; Zhu et al. 2021). Let us assume that, for the state vector (a, H, R), the field equations can be written as

$$\dot{a} = aH, \tag{71}$$

$$\dot{H} = \frac{1}{6}\left(R - 12H^2\right), \tag{72}$$

$$\dot{R} = g(a, H, R), \tag{73}$$

such that the function $g(a, H, R)$ satisfies $g(a, H, R) = -g(a, -H, R)$. Hence, the system (71)–(73) is invariant under time inversion $t \mapsto -t$ if also $H \mapsto -H$ and $R \mapsto R$, and by definition $a \geq 0$. Those solutions can be related to symmetric cyclic solutions with respect to the origin, chosen to correspond to the possible bounce point $t_{\text{bounce}} = 0$. Therefore, if the bounce exists, the system (71)–(73) is a reversible system in the sense that it has a reversing symmetry under time inversion.

Let us consider the simplest case where there is exactly one bouncing and exactly one turnaround point. Note that both at the bounce and turnaround points we have $H = 0$. In this case, the line connecting these points and corresponding to $H = 0$ defines a plane that separates all points on the trajectory in this phase space to the ones corresponding to either the expanding ($H > 0$) or contracting ($H < 0$) phase. As discussed in Pavlović & Sossich (2021), it is natural that in cyclic models the value of the Ricci scalar would approach its maximum around the bounce and since $\dot{H} > 0$, from equation (72), it follows that this maximum Ricci scalar value is positive, and moreover that $\ddot{H} = 0$ at the bounce.

In summary, at the bounce, we have $R = R_{\text{bounce}} > 0$, $H = 0$, and $a = a_{\text{min}}$. The bounce is then followed by a phase in which $\dot{H} > 0$, $H > 0$, $\dot{a} > 0$, and $\dot{R} < 0$. Then, the Universe enters the phase characterized by $\dot{H} < 0$ and approaches the turnaround point, which is determined by $H = 0$, $a = a_{\text{max}}$, and $R = R_{\text{turnaround}} < 0$, where the last condition follows from equation (72).

To obtain $g(a, H, R)$ in equation (73), we use equations (8), (9), (11), (12), and (14), where for simplicity we focus on the dust case. Therefore, we obtain

$$
\begin{aligned}
R = 6\dot{H} + 12H^2 &= -24\pi G p_{\text{DE}} \\
&= 3\bigg\{-8\pi G\rho_m\left[\text{sech}\left(\frac{\beta H_0^2}{H^2}\right) - 1\right] \\
&\quad + 3\beta H_0^2 \text{shi}\left(\frac{H_0^2\beta}{H^2}\right) - 3H^2\left[\cosh\left(\frac{\beta H_0^2}{H^2}\right) - 1\right] + \Lambda\bigg\}.
\end{aligned}
\tag{74}
$$

Introducing the dimensionless quantities $E = \frac{H}{H_0}$ and $\mathcal{R} = \frac{R}{12H_0^2}$, and using z as the independent variable, we extract the general system for $(a, E, \mathcal{R})$:

$$\frac{da}{dz} = -a^2, \tag{75}$$

$$\frac{dE}{dz} = -2\left(\mathcal{R} - E^2\right)\frac{a}{E}, \tag{76}$$

$$\frac{d\mathcal{R}}{dz} = -\frac{9\beta\Omega_m^{(0)2}\tanh\left(\frac{\beta}{E^2}\right)\text{sech}^2\left(\frac{\beta}{E^2}\right)}{4E^4a^5}. \tag{77}$$

Finally, in order to examine whether the above requirements are fulfilled in the present scenario, we use the best-fitting values $\beta = -0.011$ and $\Omega_m^{(0)} = 0.283$ in equations (75)–(77), and we find

$$\frac{da}{dz} = -a^2, \tag{78}$$

$$\frac{dE}{dz} = -2\left(\mathcal{R} - E^2\right)\frac{a}{E}, \tag{79}$$

$$\frac{d\mathcal{R}}{dz} = -\frac{0.0019822\tanh\left(\frac{0.011}{E^2}\right)\text{sech}^2\left(\frac{0.011}{E^2}\right)}{E^4a^5}. \tag{80}$$

In the case of dust matter and $\Lambda \neq 0$, this system cannot satisfy the above requirements, and hence the present scenario cannot exhibit bounce and turnaround solutions.

4.2 Case II: $\Lambda = 0$

In the case $\Lambda = 0$, equation (10) becomes

$$\frac{8\pi G\rho_m}{3H^2} = -\frac{3\pi K\,\text{shi}\left(\frac{K\pi}{GH^2}\right)}{3GH^2} + \cosh\left(\frac{\pi K}{GH^2}\right). \tag{81}$$

This expression is used as a definition of ρ_m. If $\beta \neq 0$, and rescaling the time derivative $d/d\nu = (1 - T)d/d\tau$, we obtain

$$T'(\nu) = \frac{3}{2}(1 - T)^2 T \cosh\left(\frac{\beta T^2}{(1 - T)^2}\right) - \frac{3}{2}\beta T^3 \text{shi}\left(\frac{T^2\beta}{(1 - T)^2}\right). \tag{82}$$

The equilibrium points of equation (82) are $T = 0$, which is unstable, and the equilibrium point $T = T_c$, where T_c is a solution of the transcendental equation $(1 - T_c)^2 \cosh\left(\beta T_c^2/(1 - T_c)^2\right) - \beta T_c^2 \text{shi}\left(T_c^2\beta/(1 - T_c)^2\right) = 0$, $0 < T_c < 1$, corresponding to the de Sitter solution $a(t) \propto e^{H_0 t\left(\frac{1}{T_c} - 1\right)}$, is stable. In Fig. 8, we depict a phase-space plot of the 1D dynamical system (82) of Kaniadakis horizon-entropy cosmology with $\Lambda = 0$, for dust matter, and the join value $\beta = 1.161$. Note that all orbits originate from the invariant subset $T = 0$, classically related to the initial singularity with $H \to \infty$. The late-time attractor is $T = T_c \approx 0.521$, and it corresponds to a de Sitter solution.

Finally, in order to examine whether the present scenario exhibits a bounce, we use the best-fitting values $\beta = 1.161$ and $\Omega_m^{(0)} = 0.326$ in equations (75)–(77), and we find

$$\frac{da}{dz} = -a^2, \tag{83}$$

$$\frac{dE}{dz} = -2\left(\mathcal{R} - E^2\right)\frac{a}{E}, \tag{84}$$

$$\frac{d\mathcal{R}}{dz} = \frac{0.277619\tanh\left(\frac{1.161}{E^2}\right)\text{sech}^2\left(\frac{1.161}{E^2}\right)}{E^4a^5}. \tag{85}$$

In the case of dust matter and $\Lambda = 0$, we deduce that the system cannot fulfil the bounce requirements, and therefore it cannot exhibit bounce and turnaround solutions.
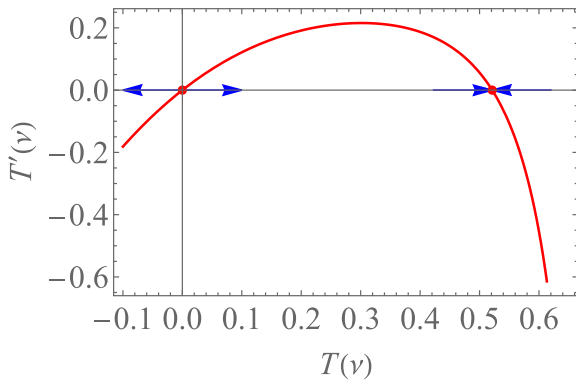
Figure 8. Phase-space diagram of the 1D dynamical system (82) of Kaniadakis horizon-entropy cosmology with $\Lambda = 0$, for dust matter and for the best-fitting value of Kaniadakis parameter obtained by the observational analysis, namely for $\beta = 1.161$. The physical region is $0 \leq T < 1$. The equilibrium point $T = 0$ is unstable, dominated by dark energy, and the de Sitter equilibrium point $T = T_c \approx 0.521$ is stable.

5 SUMMARY AND DISCUSSION

This work was devoted to explore Kaniadakis horizon-entropy cosmology, which arises from the application of the gravity-thermodynamics conjecture using the Kaniadakis modified entropy. The resulting modified Friedmann equations contain extra terms that constitute an effective dark energy sector. Moreover, we used data from OHD, SNIa, HIIG, SLSs, and BAO observations, and we applied a Bayesian MCMC analysis in order to construct the likelihood contours for the model parameters.

Regarding the Kaniadakis parameter β, we found that it is constrained around 0, namely around the value in which standard Bekenstein–Hawking is recovered. Furthermore, the present matter density parameter $\Omega_m^{(0)}$ is consistent with the expected value from the ΛCDM scenario, having a lower value for the $\Lambda \neq 0$ case and a slightly higher value for the $\Lambda = 0$ case.

However, the interesting result comes from the constraint on the normalized Hubble parameter h. In particular, for $\Lambda \neq 0$, we extracted $h = 0.708^{+0.012}_{-0.011}$, while for $\Lambda = 0$, we found $h = 0.715^{+0.012}_{-0.012}$. Thus, the obtained value of H_0 for $\Lambda \neq 0$ deviates 2.67σ from the Planck value and 1.74σ from the SH0ES one, while in the $\Lambda = 0$ case, the deviation is 3σ from the Planck value and 1.36σ from the SH0ES one. Additionally, in order to verify this result in an independent way, we performed the $\mathbb{H}0(z)$ diagnostic. Hence, our analysis reveals that Kaniadakis horizon-entropy cosmology is an interesting candidate to alleviate the H_0 tension problem. This is one of the main results of this work.

We proceeded by investigating the cosmographic parameters, namely the deceleration and jerk ones, by using the data in order to reconstruct them in the redshift region $0 < z < 2.5$. As we showed, the transition from deceleration to acceleration happens at $z_T = 0.715^{+0.042}_{-0.041}$ for the $\Lambda \neq 0$ case and at $z_T = 0.652^{+0.032}_{-0.031}$ for the $\Lambda = 0$ case, in agreement within 1σ with that found in Herrera-Zamorano, Hernández-Almada & García-Aspeitia (2020) for ΛCDM cosmology. Furthermore, we applied the AICc and BIC information criteria, and we found that although AICc suggests that $\Lambda \neq 0$ model and ΛCDM are statistically equivalent in the joint analysis, BIC indicates that there is strong evidence against the candidate model. Lastly, applying the DIC criterion, we found that the $\Lambda \neq 0$ case and ΛCDM are statistical equivalent for BAO, they have a moderate tension for OHD and SLS, and a strong tension for HIIG and SNIa

data sets, while the $\Lambda \neq 0$ case and ΛCDM are statistical equivalent for all data sets.

Finally, we performed a detailed dynamical system analysis, providing a general description of the phase space of all possible solutions of the system, their equilibrium points and stability, as well as the late-time asymptotic behaviour. As we showed, the Universe past attractor is the matter-dominated epoch, while at late times, the Universe results in the dark-energy-dominated solution, for both $\Lambda = 0$ and $\Lambda \neq 0$ cases. Moreover, we showed that the scenario accepts heteroclinic sequences, but it cannot lead to bounce and turnaround solutions.

In summary, the scenario of Kaniadakis horizon-entropy cosmology exhibits very interesting phenomenology and is in agreement with observational behaviour. Hence, it can be an interesting candidate for the description of nature.

DATA AVAILABILITY

The data underlying this paper were cited in Section 3.1.

REFERENCES

Abreu E. M. C., Ananias Neto J., 2021, Europhys. Lett., 133, 49001
Abreu E. M. C., Ananias Neto J., Barboza E. M., Nunes R. C., 2016, Europhys. Lett., 114, 55001
Abreu E. M. C., Ananias Neto J., Mendes A. C. R., Bonilla A., 2018, Europhys. Lett., 121, 45002
Addazi A. et al., 2021, Progress in Particle and Nuclear Physics, preprint (arXiv:2111.05659)
Aghanim N. et al., 2020, A&A, 641, A6
Akaike H., 1974, IEEE Trans. Autom. Control, 19, 716
Akbar M., Cai R.-G., 2006, Phys. Lett. B, 635, 7
Akbar M., Cai R.-G., 2007, Phys. Rev. D, 75, 084003
Amante M. H., Magaña J., Motta V., García-Aspeitia M. A., Verdugo T., 2020, MNRAS, 498, 6013
Asimakis P., Basilakos S., Mavromatos N. E., Saridakis E. N., 2021, preprint (arXiv:2112.10863)
Bak D., Rey S.-J., 2000, Class. Quant. Grav., 17, L83
Barrow J. D., 2020, Phys. Lett. B, 808, 135643
Barrow J. D., Basilakos S., Saridakis E. N., 2021, Phys. Lett. B, 815, 136134

Beutler F. et al., 2011, MNRAS, 416, 3017
Blake C. et al., 2011, MNRAS, 418, 1707
Cai R.-G., Cao L.-M., 2007, Phys. Rev. D, 75, 064008
Cai R.-G., Kim S. P., 2005, JHEP, 02, 050
Cai R.-G., Ohta N., 2010, Phys. Rev. D, 81, 084061
Cai R.-G., Cao L.-M., Hu Y.-P., 2009, Class. Quant. Grav., 26, 155018
Cai Y.-F., Gao C., Saridakis E. N., 2012, J. Cosmol. Astropart. Phys., 10, 048
Capozziello S., Lambiase G., Saridakis E. N., 2017, Eur. Phys. J. C, 77, 576
Carroll S. M., 2001, Living Rev. Relativ., 4, 1
Chen X.-m., Gong Y.-g., Saridakis E. N., 2009, J. Cosmol. Astropart. Phys., 04, 001
Chen L., Huang Q.-G., Wang K., 2019, J. Cosmol. Astropart. Phys., 02, 028
Coley A. A., 2003, Dynamical Systems and Cosmology, Vol. 291. Springer, Dordrecht
Copeland E. J., Liddle A. R., Wands D., 1998, Phys. Rev. D, 57, 4686
Copeland E. J., Sami M., Tsujikawa S., 2006, Int. J. Mod. Phys. D, 15, 1753
Cotsakis S., Kittou G., 2013, Phys. Rev. D, 88, 083514
Drepanou N., Lymperis A., Saridakis E. N., Yesmakhanova K., 2021, preprint (arXiv:2109.09181)
Fan Z.-Y., Lu H., 2015, Phys. Rev. D, 91, 064009
Ferreira P. G., Joyce M., 1997, Phys. Rev. Lett., 79, 4740
Foreman-Mackey D., Hogg D. W., Lang D., Goodman J., 2013, PASP, 125, 306
Frolov A. V., Kofman L., 2003, J. Cosmol. Astropart. Phys., 05, 009
García-Aspeitia M. A., Hernández-Almada A., 2021, Phys. Dark Univ., 32, 100799
Garcia-Aspeitia M. A., Hernandez-Almada A., Magaña J., Amante M. H., Motta V., Martínez-Robles C., 2018, Phys. Rev. D, 97, 101301
García-Aspeitia M. A., Martínez-Robles C., Hernández-Almada A., Magaña J., Motta V., 2019, Phys. Rev. D, 99, 123525
García-Aspeitia M. A., Hernández-Almada A., Magaña J., Motta V., 2021, Phys. Dark Univ., 32, 100840
Giambo R., Miritzis J., 2010, Class. Quant. Grav., 27, 095003
Gibbons G. W., Hawking S. W., 1977, Phys. Rev. D, 15, 2738
Gim Y., Kim W., Yi S.-H., 2014, JHEP, 07, 002
Giostri R., dos Santos M. V., Waga I., Reis R., Calvão M., Lago B. L., 2012, J. Cosmol. Astropart. Phys., 03, 027
González-Morán A. L. et al., 2021, MNRAS, 505, 1441
Guckenheimer J., Holmes P., 1983, Applied Mathematical Sciences, vol. 42, Nonlinear Oscillations, Dynamical Systems, and Bifurcations of Vector Fields. Springer, New York
Hernández-Almada A., Magaña J., García-Aspeitia M. A., Motta V., 2019, Eur. Phys. J. C, 79, 12
Hernández-Almada A., Leon G., Magaña J., García-Aspeitia M. A., Motta V., Saridakis E. N., Yesmakhanova K., 2022, MNRAS, 511, 4147
Herrera-Zamorano L., Hernández-Almada A., García-Aspeitia M. A., 2020, Eur. Phys. J. C, 80, 637
Hurvich C. M., Tsai C. L., 1989, Biometrika, 76, 297
Jacobson T., 1995, Phys. Rev. Lett., 75, 1260
Jamil M., Saridakis E. N., Setare M. R., 2010a, J. Cosmol. Astropart. Phys., 11, 032
Jamil M., Saridakis E. N., Setare M. R., 2010b, Phys. Rev. D, 81, 023007
Jeffreys H., 1961, Theory of Probability, 3rd edn., Clarendon Press, Oxford
Kaniadakis G., 2002, Phys. Rev. E, 66, 056125
Kaniadakis G., 2005, Phys. Rev. E, 72, 036108

Krishnan C., Ó Colgáin E., Sheikh-Jabbari M., Yang T., 2021, Phys. Rev. D, 103, 103509
Kunz M., Trotta R., Parkinson D. R., 2006, Phys. Rev. D, 74, 023503
Leon G., Magaña J., Hernández-Almada A., García-Aspeitia M. A., Verdugo T., Motta V., 2021, J. Cosmol. Astropart. Phys., 12, 032
Liddle A., 2007, MNRAS, 377, L74
Lymperis A., Saridakis E. N., 2018, Eur. Phys. J. C, 78, 993
Lymperis A., Basilakos S., Saridakis E. N., 2021, Eur. Phys. J. C, 81, 1037
Lyra M. L., Tsallis C., 1998, Phys. Rev. Lett., 80, 53
Moradpour H., Ziaie A. H., Kord Zangeneh M., 2020, Eur. Phys. J. C, 80, 732
Moresco M. et al., 2016, J. Cosmol. Astropart. Phys., 05, 014
Motta V., García-Aspeitia M. A., Hernández-Almada A., Magaña J., Verdugo T., 2021, Universe, 7, 163
Nadathur S., Percival W. J., Beutler F., Winther H., 2020, Phys. Rev. Lett., 124, 221301
Padmanabhan T., 2005, Phys. Rep., 406, 49
Padmanabhan T., 2010, Rep. Prog. Phys., 73, 046901
Papagiannopoulos G., Basilakos S., Saridakis E. N., 2022, preprint (arXiv:2202.10871)
Paranjape A., Sarkar S., Padmanabhan T., 2006, Phys. Rev. D, 74, 104015
Pavlović P., Sossich M., 2021, Phys. Rev. D, 103, 023529
Percival W. J. et al., 2010, MNRAS, 401, 2148
Perko L., 2000, Differential Equations and Dynamical Systems, 3rd edn., Springer, New York
Pospelov M., Pradler J., 2010, Annu. Rev. Nucl. Part. Sci., 60, 539
Riess A. G. et al., 1998, AJ, 116, 1009
Riess A. G., Casertano S., Yuan W., Macri L. M., Scolnic D., 2019, ApJ, 876, 85
Riess A. G., Casertano S., Yuan W., Bowers J. B., Macri L., Zinn J. C., Scolnic D., 2021, ApJ, 908, L6
Saridakis E. N., 2009, Nucl. Phys. B, 808, 224
Saridakis E. N., 2020, J. Cosmol. Astropart. Phys., 07, 031
Saridakis E. N., Basilakos S., 2021, Eur. Phys. J. C, 81, 7
Saridakis E. N. et al., 2021, preprint (arXiv:2105.12582)
Schwarz G., 1978, Ann. Stat., 6, 461
Scolnic D. M. et al., 2018, ApJ, 859, 101
Sheykhi A., 2010a, Eur. Phys. J. C, 69, 265
Sheykhi A., 2010b, Phys. Rev. D, 81, 104011
Sheykhi A., 2018, Phys. Lett. B, 785, 118
Sheykhi A., Wang B., Cai R.-G., 2007, Nucl. Phys. B, 779, 1
Spergel D. N. et al., 2003, ApJS, 148, 175
Spiegelhalter D. J., Best N. G., Carlin B. P., Van Der Linde A., 2002, J. R. Stat. Soc. B (Stat. Methodol.), 64, 583
Sugiura N., 1978, Commun. Stat. - Theory Methods, 7, 13
Tsallis C., 1988, J. Stat. Phys., 52, 479
Wainwright J., Ellis G. F. R., 1997, Dynamical Systems in Cosmology. Cambridge Univ. Press, Cambridge
Wang M., Jing J., Ding C., Chen S., 2010, Phys. Rev. D, 81, 083006
Weinberg S., 1989, Rev. Mod. Phys., 61, 1
Zel'dovich Y., Krasinski A., Zeldovich Y., 1968, Sov. Phys. Usp., 11, 381
Zhu M., Ilyas A., Zheng Y., Cai Y.-F., Saridakis E. N., 2021, J. Cosmol. Astropart. Phys., 11, 045

This paper has been typeset from a TEX/LATEX file prepared by the author.